Indonesian Journal of Electrical Engineering and Computer Science
Vol. 24, No. 1, October 2021, pp. 245~252
ISSN: 2502-4752, DOI: 10.11591/ijeecs.v24.i1.pp245-252

Bone cancer detection using electrical impedance tomography

Nabanita Saha, Mohammad Anisur Rahaman
Department of Electronics and Telecommunication Engineering, Chittagong University of Engineering and Technology, Chittagong, Bangladesh

Article Info

Article history:

Received Feb 1, 2021
Revised Jul 19, 2021
Accepted Aug 4, 2021

Keywords:

EIDORS
Electrical impedance tomography
Image reconstruction algorithms
MATLAB
Simulation

ABSTRACT

Bone cancer is an uncommon sort of malignancy that alludes to irregular development of tissue inside the bone, with high opportunity to spread to different pieces of the body. It is extremely important to distinguish bone cancer at the beginning phase to cure it productively. Presently, in addition to a physical examination, magnetic resonance imaging, blood tests, positron emission tomography (PET), computed tomography (CT) or PET-CT scan, X-ray, Bone scan, Biopsy and computed tomography scan, are used to diagnose or determine the stage (or extent) of bone sarcoma. But these methods are costly and not free of radiation. Moreover, these machines are bulky. Electrical impedance tomography approach was proposed in this research for identifying bone cancer as this detection technique is able to distinguish between cancerous and non-cancerous cells by differentiating between their conductivity and it has the possibility to remove the limitations of conventional medical imaging techniques. Here, equivalent bone models were generated using (electrical impedance and diffused optical reconstruction software (EIDORS) which had been implemented in MATLAB, and three different image reconstruction algorithms-GREIT, Sheffield Backprojection, Gauss-Newton inverse algorithm had been used to detect the cancerous cells.

Corresponding Author:

Nabanita Saha
Department of Electronics and Telecommunication Engineering
Chittagong University of Engineering and Technology
Kaptai, Highway Raozan Pahartali Rd, Chattogram 4349
Email: u1508020@student.cuet.ac.bd

1. INTRODUCTION

Cancer is a threatening disease which refers to a malignant growth or tumor resulting from an uncontrolled division of cells and affects nearby parts of the body. Tumors in a bone generate while the bone cells split uncontrollably and form a cluster of tissue. As per the U.S. Surveillance, epidemiology and end results program [1], osteosarcomas contribute 36% of a wide range of bone malignant growth, trailed by chondrosarcomas and Ewing's sarcomas with around 30% and 16% distinctly. Bone malignant growth can start in any bone in the body, yet it ordinarily impacts the pelvis or the long bones of the arms and legs. There are mainly two sorts of bone cancer and they are primary bone cancer and secondary bone cancer. Primary bone cancer occurs in the bone. Secondary bone cancerwhen malignant growth has spread to the bones from where it began. The reasons of bone cancer have not been clearly recognized. However, acquired hereditary transformations, radiation, injury, have been recognized as potential causes. The American Cancer Society's evaluations for malignant growth of the bones and joints for 2020 are:

– About 3,600 new cases will be analyzed
– About 1,720 passings from these diseases are predictable

Ordinary clinical imaging procedures either utilize destructive radiations that might be harmful to the body tissues or the expense isn't reasonable to all. The machines are not compact. As a clinical imaging methodology, electrical impedance tomography (EIT) offers to solve these problems: the non-intrusive connection to a patient with electrodes and wires is appropriate for ceaseless intensive care applications; it is free of hazardous radiation; this is fit for operating at high casing rates providing great transient resolution; this is conceivably cheap, utilizing off-the-rack low-frequency hardware parts. Then again, EIT provides a low spatial resolution,as well as is inclined to relics from terminal development and helpless contact quality [2].

EIT is a non-invasive clinical imaging strategy in which electricity is applied to the outer part of human body using contact electrodes and the subsequent surface voltages are utilized in the reproduction of pictures [3]. The conductivity of cancerous and non-cancerous cells is different and this property can be helpful for detecting cancer [4]. EIT is able to be helpful to implementations where conductive differences exist between cluster of tissues, liquids, or vapors, for example, imaging of destructive or ischemic tissue or utilitarian checking of inhalation, neural movement, bloodstream, and intestinal motility [4]. EIT illustrates a structural image of the dissemination of conductance. It has been being used in medical purposes in the late 1970s [5] and mid 1980s [6]. Numerous clinical uses have been suggested for EIT such as in recruitment/derecruitment of lung tissue [7], contrast-based perfusion measurement [8], screening of breast cancer [9], [10], Prostate cancer screening [11], [12], gastric and Intestinal motility [13], cerebral perfusion [14], titrate positive end-expiratory pressure in COVID-19 acute respiratory distress syndrome [15]. In the field of detecting bone cancer, electrical impedance tomography is a new method.

Bone cancer is an unusual kind of malignancy that structures as an excruciating lump (‘tumor’) in human bone. This is otherwise called bone sarcoma. While bone malignancy originates in the body, the carcinogenic cells increase and begin to devastate human bone. There are different approaches for depicting bone cancer using image processing such as k-means segmentation and knn classification [16]. A restricted version of EIT named enclosure method to extract stable features from the data and convolutional neural network can be used also [17]. A computed tomography (CT) image-guided electrical impedance tomography (EIT) method for clinical imaging can be implemented too [18]. Benign cancer tumor is equivalent to non-conducting impurity while the malignant tumor is equivalent to conducting impurity. The normal tissue and the cancerous show different conductivity and dielectric properties. Malignant tumors show expanded capacitance and conductance esteems hence decline its impedance [19]. The benign tissue and the malignant tumors are different according to their conductivity: close-to 35 micro siemens/mm for normal bone tissue and 3-4 times greater for cancerous tissue at 1 kHz [20]. The impedance contrast is more articulated at higher frequencies, cresting at roughly 1 MHz [20]. These contrasts will permit to separate between the typical tissue and harmful tissue. EIDORS is utilized for 2-D and 3-D reconstruction of images according to voltage datasets. EIDORS is an open-source suite executed in MATLAB package [21], [22]. This software is partitioned into three phases i.e. mesh generation, forward problem, and inverse problem [23]. In the explanation of inverse problem, the applied electricity rate and the voltage on the edge, calculated with electrodes are utilized for evaluating the reckoned internal dissemination of resistivity [24].

2. THE PROPOSED METHOD

The mechanism of detecting tumor or cancerous cell can be illustrated. These steps are contrasting electrical properties of tissues, electrodes positioning, solving the forward problem, image reconstruction (solving inverse problem) and diagnosis of tumor from EIT image as shown in Figure 1.

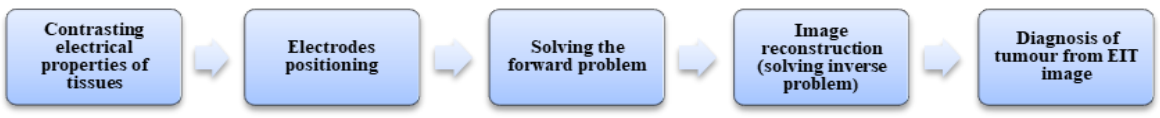

Figure 1. Image interpretation pathway by using EIT

2.1. Contrasting electrical properties of tissues

The conductivity and permittivity of the cancerous and non-cancerous tissues are different. Here is the conductivity and permittivity of healthy tissue and tumor. The constants used in these equations are introduced in Table 1. Here, s1, s2 and s3 are relative permittivity measured three times and r1, r2 and r3 are electrical conductivity measured three times. The simulations are performed in normal temperature.

Table 1. The coefficients of the temperature dependence dielectric properties [25]-[27]

	Relative permittivity			Electrical conductivity		
	S1	S2	S3	r1	r2	r3
Healthy Tissue	44.3	5.223	5.223	1.80	6.583	0.0598
Tumour	54.8	5.223	5.223	2	6.583	0.0598

The dielectric properties of the tissue are dependent on temparature [27]. The electrical permittivity (l) and electrical conductivity (S/m) is denoted by a linear function of temperature, [25], [26],

$$\text{Ɛ}(T)= s1\ [1- 1/\{1+\exp(s2-s3T)\}]$$

$$\delta(T)= r1\ [1- 1/\{1+\exp(r2-r3T)\}]$$

2.2. Electrodes positioning

Experimental arrangement of EIT incorporates a signal generator, a voltage to current converter delivering a electricity of 20 mA at 5 kHz, a phantom model of the object with 16 electrodes set up and a multimeter for the measurement of subsequent differential voltages [28]. The current can be applied in neighboring pattern. In first projection current is applied to one sets for example electrode 1 and electrode 2 and differential voltage is calculated between other pair i.e. between electrode 3 and 4 then voltage drive is moved to next pair between electrode 4 and 5 and so on up to last pair i.e. electrode 15 and 16. The electricity density is the most noteworthy between current electrodes and continues diminishing quickly as a function of distance. Round electrodes are characterized by the crossing point of the central chamber with cylinders and electrode mesh modification is executed by indicating a lesser maximum mesh size for every radial cylinder.

2.3. Solving the forward problem

The forward problem is typically solved with finite elements method (FEM) [29]. Forward problem explanation contains computation of voltage value on the superficial level electrodes for individual resistivity dissemination, while equally the resistivity dissemination of the bone and applied electricity rate are acknowledged. The forward problem is demonstrated with boundary conditions and Laplace equation by applying the FEM method [30]. In elucidation of the inverse problem the used electricity rate and the voltage value on the border, calculated with electrodes are utilized for evaluating the assessed inner dissemination of resistivity [31]. Here, a cylindrical shaped finite elements method model has been created which is reasonable for performing simulations.

2.4. Image reconstruction (solving inverse problem)

Reconstruction of image in electrical impedance tomography (EIT) is a nonlinear, ill-posed inverse problem. Here, image has been reconstructed with the "Graz consensus reconstruction algorithm for EIT (GREIT), Sheffield Backprojection, Gauss-Newton Inverse algorithm. The GREIT involves a comprehensive, homogenous technique dependent on point-formed training and assessment data. GREIT comprises of point-formed changes in the homogenous background impedance. On the off chance that we recognize the impedance-space to be discretized, we can consider these adjustments in impedance as a great deal of unit vectors. The Sheffield image reconstruction algorithm depends on the presumption that the underlying conductance appropriation of human body is uniform. One-step Gauss-Newton (GN) EIT reconstruction approaches was generally utilized in EIT (eg. Cheney *et al* 1990; Adler and Guardo, 1996). These approaches permit utilization of refined standardized models of the EIT inverse problem, can denote this solution as a linear reconstruction matrix, that would be able to permit quick, real-time imaging.

2.5. Diagnosis of tumor from EIT image

As the tumors show different electrical properties from the normal tissues, the position of the tumor can easily be detected. Applying different reconstruction methods, the tomographic image of the tumor can be compared.

3. DESIGN OF PHANTOM MODEL

A cylindrical geometry has been characterized as a human bone with the electrodes which are attached around the phantom model of the bone as shown in Figure 2. These materials have decided to carry on similarly to human tissues. No noise has been added to the simulated electrode voltage signal. This technique has not been used for bone cancer in real system yet, so the proposed mechanism for detecting

bone cancer is simulated to get the output. The code proceeds by taking the number of the electrodes (16) and the inhomogeneous materials (tumor) as inputs as shown in Figure 3.

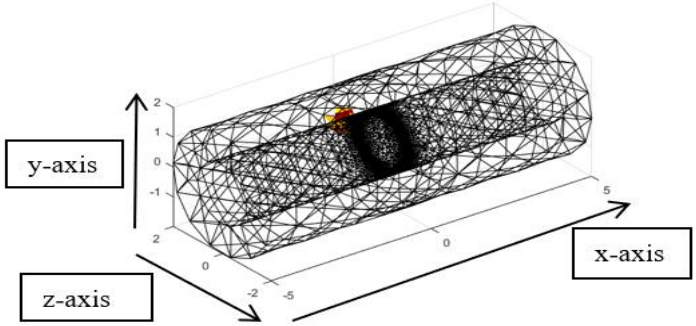

Figure 2. Human phantom model containing tumor

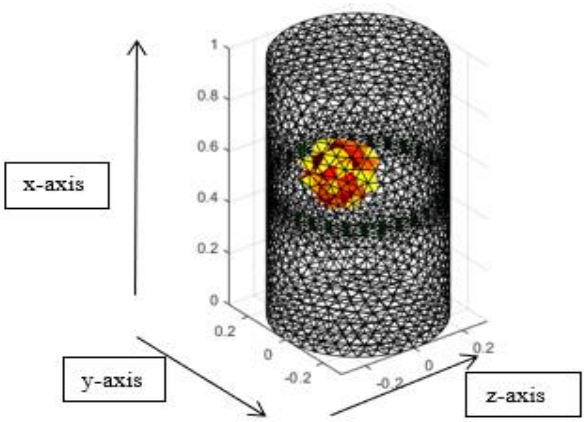

Figure 3. Applying electrodes on the surface of the phantom model

4. RESULTS AND DISCUSSIONS

In this part, it is clarified the results of the research and simultaneously is given a comprehensive discussion. This paper focuses on 2-D reconstruction in view of the location of the tumor as unidentified. 2-D EIT reconstruction image has been acquired for classification of normal and cancerous lung tissues but it has not been for bone cancer yet. Starting step for assessing the conductivity and permittivity dissemination in long bone is to generate finite element model of electrodes. This finite model is explained by expecting homogenous conductivity and computing voltage distribution. The voltage dataset is stacked in MATLAB. Inverse algorithm is implemented. Inverse algorithm utilizes distinction technique to acquire image reconstruction.

4.1. Image reconstruction using different algorithms

A bone tissue is characterized in the correct territory section, while the whole locale is portrayed as homogeneous. After simulation, reconstructed image with the GREIT, Sheffield Backprojection, Gauss-Newton Inverse algorithm is acquired and it shows the 2D framework of the tumor. We require a structure for estimating the surface calculation, a mesh generator for making a cross section dependent on a superficial level data, code for calculating the finite element estimation and a perfect algorithm for cracking the inverse problem for reconstructing EIT images in geometrical settings. We also require devices to show the outcomes and furthermore to analyze the images. The reconstruction of the image from the information acquired by EDIORS has been shown. The location of electrodes and the location of carcinogenic tissue are visibly observed in reconstructed images of EIDORS. The blue shading displays the sudden lessening of conductance. In this way the existence of conducting impurities (malignant cancer tumor) is distinguished. Also, the red tone in reproduced pictures recognizes the presence of non-conducting (benign malignancy tumor) impurity. GREIT plots the similar curios to ‘blobs’ as shown in Figure 4. This is simpler for an

administrator to determine such blobs and recognize the existence of data errors. It shows limited shape deformation of the object.

Sheffield backprojection inclines to plot measurement artifacts to 'streaks'. These streaks show the situation of the tumor and in this manner bone malignancy as shown in Figure 5. The Sheffield image reconstruction algorithm depends on the supposition that the underlying conductance dissemination of the human body is uniform. This algorithm is officially denoted as $c_n = B(FB)^{-1} g_n$ here, 'c_n' a normalized image of conductivity values ,'g_n' is a normalized boundary measurements vector, 'F' the forward transform matrix, which takes a known conductivity distribution into boundary data ($g_n = Fc_n$) given knowledge of the electricity injection pattems and 'B' a backprojection matrix [32]. Outcomes establish that the Gauss-Newton algorithm is able to precisely reconstruct the location and outline of the object, but exhibit lesser noise performance as shown in Figure 6.

The Gauss-Newton with data which is averaged obscures the reconstructed picture crosswise all the averaged data frames on the other hand, can exhibit better noise performance which is estimated from collective averaging. Thus, this algorithm is suggested when noise levels are low, when the conductivity is changing gradually concerning the frame rate, Gauss-Newton with weighted data is a better method [33].

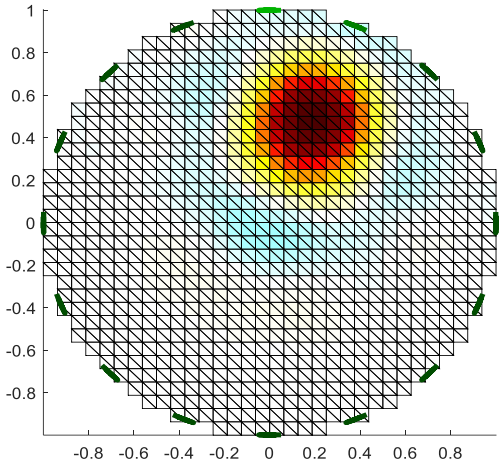

Figure 4. Reconstructed image of detecting the cancer cell using GREIT algorithm

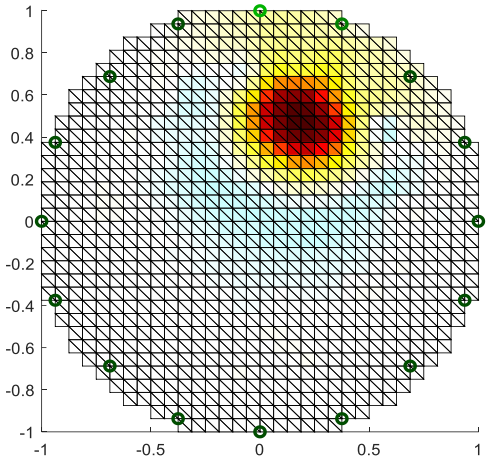

Figure 5. Reconstructed image of detecting the cancer cell using Sheffield Backprojection algorithm

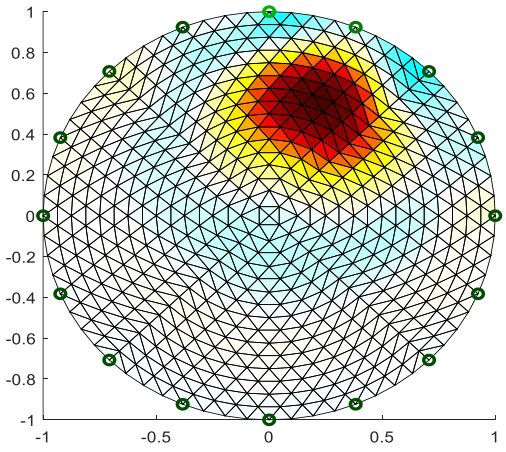

Figure 6. Reconstructed image of detecting the cancer cell using the Gauss Newton inverse algorithm

4.2. Performance comparison

The comparison between the performances of these three algorithms is shown in Figure 7. These plots show the correlation between the algorithms as shown in Figure 7. Different contemplations were made

in the wake of amassing the total EIT system. EIDORS gives an interface to test algorithm performance against the parameters characterized for the GREIT algorithm: Amplitude (AR), position error (PE), resolution (RES), shape deformation (SD), and ringing (RNG) as shown in Figure 8. The key contrast is that GREIT structure depends on a bunch of execution necessities, while other reproduction calculations depend straightforwardly on the basic numerical models that express the performance requirements expressly.

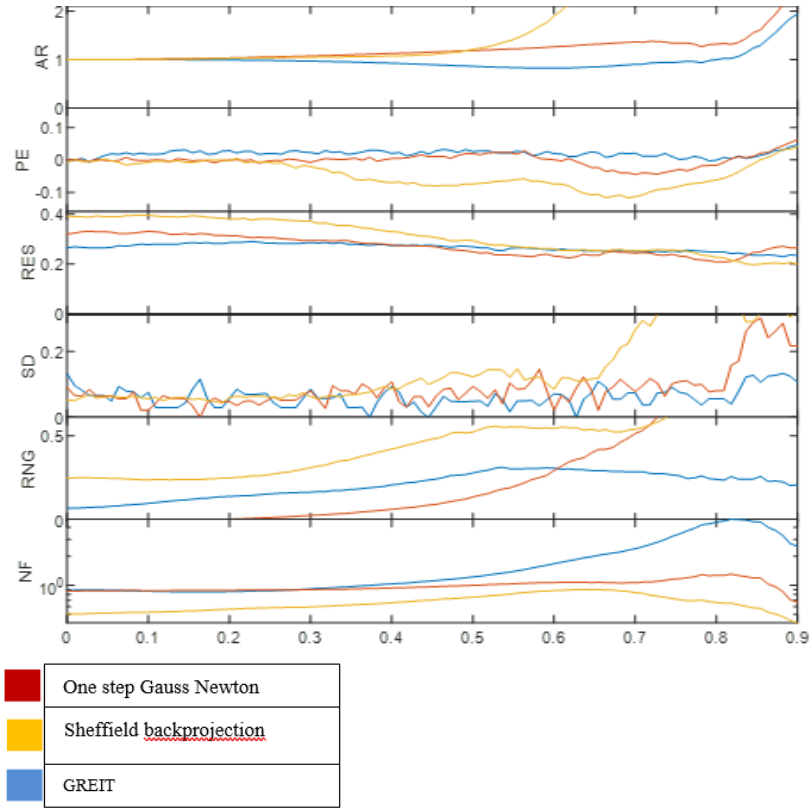

Figure 7. Performance of algorithms

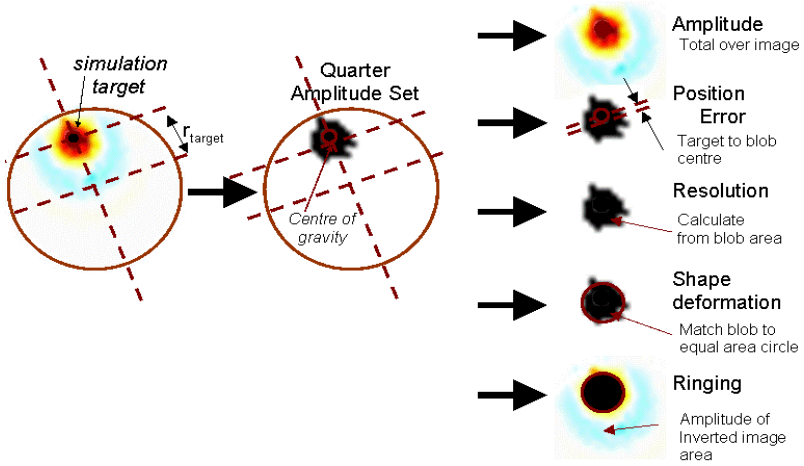

Figure 8. Parameters defined for the algorithms

Phantom tumors were properly recognized and separated from non-destructive tissue based on impedance. In ampliitude and phase at 1 kHz and 100 kHz, the areas of low impedance tumor distinguished

had impedance contrasts from the normal tissue larger than the standard deviation in impedance in the tumor position. In Sheffield Backprojection and Gauss-Newton, the reconstructed images illustrate spatial non-consistency in the amplitude of image, location, and resolution, which make explanation of regional air circulation tough and error-prone. GREIT method does not introduce such problems. Sheffield back-projection performs well for objects on which are far from the medium limit; close to the boundary, it creates smearing artifacts. GN reconstruction creates perfect ringing artifacts, yet in any case illustrates great execution with perfect resolution. A little lesser resolution than Gauss-Newton algorithm is provided by GREIT, yet this algorithm provides more steady resolution with so small ringing artefacts, keeping similar to the consensus prerequisites [33]. Gauss-Newton algorithm gives us better reconstructred pictures regarding shape and size of tumour. A drawback of Sheffield backprojection reconstruction algorithm is that it is a hindrance to interpretation of EIT images since the reconstructed images are not described well. This issue can be solved by GREIT method.

5. CONCLUSION

As electrical impedance tomography is a cost-effective and radition-free method for patients, it has the probabilities of taking place of the other medical imaging techniques in near future. The development of different algorithms for reconstruction of images is an important part of the research. In this research, three different algorithms have been tested and verified on a phantom model of bone and their performance is compared precisely to identify their suitability in different conditions. The limitations of Sheffield backprojection and Gauss-Newton reconstruction algorithm can be solved by GREIT algorithm. These observations are feasible able to open a new era in the detection of bone cancer. It is an ongoing project and it can be applied to a real bone in future. In future, noise removal from the voltage signal can be done. Some study to identify the false positives and remove these problems can be done also in future for getting accurate result.

REFERENCES

[1] B. K. Edwards, *et al.*, "Annual report to the nation on the status of cancer, 1975-2006, featuring colorectal cancer trends and impact of interventions (risk factors, screening, and treatment) to reduce future rates," *Cancer*, vol. 116, no. 3, pp. 544-573, 2010, doi: 10.1002/cncr.24760.

[2] A. Adler and A. Boyle, "Electrical Impedance Tomography: Tissue Properties to Image Measures," *IEEE Transactions on Biomedical Engineering*, vol. 64, no. 11, pp. 2494-2504, 2017, doi: 10.1109/TBME.2017.2728323.

[3] V. Sarode, P. M. Chimurkar, and A. N. Cheeran, "Electrical Impedance Tomography (Eit) Based Medical Imaging Using Finite Element Method (Fem)," *Int. J. Eng. Sci. Emerg. Technol.*, vol. 1, no. 2, pp. 83-89, 2012, doi: 10.7323/ijeset/v1_i2_10.

[4] M. Al Ahmad, Z. Al Natour, F. Mustafa, and T. A. Rizvi, "Electrical Characterization of Normal and Cancer Cells," *IEEE Access*, vol. 6, no. c, pp. 25979-25986, 2018, doi: 10.1109/ACCESS.2018.2830883.

[5] R. P. Henderson and J. G. Webster, "An Impedance Camera for Spatially Specific Measurements of the Thorax," *IEEE Trans. Biomed. Eng.*, vol. BME-25, no. 3, pp. 250-254, 1978, doi: 10.1109/TBME.1978.326329.

[6] S. Smith, H. Wu, and J. Jia, "Low Cost Instrumentation for Electrical Impedance Tomography in Biomedical Applications," *ScienceOpen Posters*, 2015, doi: 10.14293/P2199-8442.1.SOP-ENG.PSMGXT.v1.

[7] I. Frerichs, P. A. Dargaville, T. Dudykevych, and P. C. Rimensberger, "Electrical impedance tomography: A method for monitoring regional lung aeration and tidal volume distribution?," *Intensive Care Med.*, vol. 29, no. 12, pp. 2312-2316, 2003, doi: 10.1007/s00134-003-2029-z.

[8] I. Frerichs *et al.*, "Regional lung perfusion as determined by electrical impedance tomography in comparison with electron beam CT imaging," *IEEE Trans. Med. Imaging*, vol. 21, no. 6, pp. 646-652, 2002, doi: 10.1109/TMI.2002.800585.

[9] M. Assenheimer *et al.*, "The T-SCANTM technology: electrical impedance as a diagnostic tool for breast cancer detection," *Physiol. Meas.*, vol. 22, no. 1, pp. 1-8, 2001.

[10] V. Cherepenin *et al.*, "A 3D electrical impedance tomography (EIT) system for breast cancer detection," *Physiol. Meas.*, vol. 22, no. 1, pp. 9-18, 2001, doi: 10.1088/0967-3334/22/1/302.

[11] A. Borsic, R. Halter, Y. Wan, A. Hartov, and K. D. Paulsen, "Sensitivity study and optimization of a 3D electric impedance tomography prostate probe," *Physiol. Meas.*, vol. 30, no. 6, 2009, doi: 10.1088/0967-3334/30/6/S01.

[12] R. J. Halter, A. Hartov, J. A. Heaney, K. D. Paulsen, and A. R. Schned, "Electrical impedance spectroscopy of the human prostate," *IEEE Trans. Biomed. Eng.*, vol. 54, no. 7, pp. 1321-1327, 2007, doi: 10.1109/TBME.2007.897331.

[13] H. Search, C. Journals, A. Contact, M. Iopscience, and I. P. Address, "Applied potential tomography : a new noninvasive technique for assessing gastric function," *Clinical Physics and Physiological Measurement*, vol. 8, no. 4A, 1987, doi: 10.1088/0143-0815/8/4A/016.

[14] A. Adler, M. Faulkner, K. Aristovich, S. Hannan, J. Avery, and D. Holder,"Cerebral perfusion imaging using EIT", *Proceedings of the 18th International Conference on Biomedical Applications of Electrical Impedance Tomography*, Thayer School of Engineering at Dartmouth Hanover, New Hampshire, USA, June 21-24, 2017, pp. 1-12.

[15] F. Perier *et al.*, "Electrical impedance tomography to titrate positive end-expiratory pressure in COVID-19 acute respiratory distress syndrome," *Crit. Care*, vol. 24, no. 1, pp. 1-9, 2020, doi: 10.1186/s13054-020-03414-3.
[16] M. M. Ranjitha, L. Taranath N, N. Arpitha N, C. K. Subbaraya, "Bone Cancer Detection Using K-Means Segmentation And Knn Classification," *2019 1st International Conference on Advances in Information Technology (ICAIT)*, 2019, pp. 76-80, doi: 10.1109/ICAIT47043.2019.8987328.
[17] S. Siltanen and T. Ide, "Electrical impedance tomography, enclosure method and machine learning," *IEEE Int. Work. Mach. Learn. Signal Process. MLSP*, vol. 2020-September, no. 3, pp. 6-11, 2020, doi: 10.1109/MLSP49062.2020.9231717.
[18] Z. Li, J. Zhang, D. Liu, and J. Du, "CT Image-Guided Electrical Impedance Tomography for Medical Imaging," *IEEE Trans. Med. Imaging*, vol. 39, no. 6, pp. 1822-1832, 2020, doi: 10.1109/TMI.2019.2958670.
[19] J. Jossinet, "The impedivity of freshly excised human breast tissue," *Physiol. Meas.*, vol. 19, no. 1, pp. 61-75, 1998, doi: 10.1088/0967-3334/19/1/006.
[20] B. Scholz and R. Anderson, "On electrical impedance scanning - principles and simulations," *Electromedica*, vol. 68, pp. 35-44, 2000.
[21] A. Adler and W. R. B. Lionheart, "EIDORS: Towards a community-based extensible software base for EIT," *6th Conf. Biomed. Appl. Electr. Impedance Tomogr. London, UK*, 2005, pp. 1-4.
[22] A. Adler and W. R. B. Lionheart, "Uses and abuses of EIDORS: An extensible software base for EIT," *Physiol. Meas.*, vol. 27, no. 5, 2006, doi: 10.1088/0967-3334/27/5/S03.
[23] M. Vauhkonen, W. R. B. Lionheart, L. M. Heikkinen, P. J. Vauhkonen, and J. P. Kaipio, "A MATLAB package for the EIDORS project to reconstruct two-dimensional EIT images," *Physiol. Meas.*, vol. 22, no. 1, pp. 107-111, 2001, doi: 10.1088/0967-3334/22/1/314.
[24] X. Zhang *et al.*, "A numerical computation forward problem model of electrical impedance tomography based on generalized finite element method," *IEEE Trans. Magn.*, vol. 50, no. 2, pp. 1045-1048, 2014, doi: 10.1109/TMAG.2013.2285161.
[25] Z. Ji and C. L. Brace, "Expanded modeling of temperature-dependent dielectric properties for microwave thermal ablation," *Phys. Med. Biol.*, vol. 56, no. 16, pp. 5249-5264, 2011, doi: 10.1088/0031-9155/56/16/011.
[26] V. Lopresto, R. Pinto, and M. Cavagnaro, "Experimental characterisation of the thermal lesion induced by microwave ablation," *Int. J. Hyperth.*, vol. 30, no. 2, pp. 110-118, 2014, doi: 10.3109/02656736.2013.879744.
[27] A. P. O'Rourke *et al.*, "Dielectric properties of human normal, malignant and cirrhotic liver tissue: In vivo and ex vivo measurements from 0.5 to 20 GHz using a precision open-ended coaxial probe," *Phys. Med. Biol.*, vol. 52, no. 15, pp. 4707-4719, 2007, doi: 10.1088/0031-9155/52/15/022.
[28] T. K. Bera and J. Nagaraju, "Resistivity imaging of a reconfigurable phantom with circular inhomogeneities in 2D-electrical impedance tomography," *Meas. J. Int. Meas. Confed.*, vol. 44, no. 3, 2011, pp. 518-526, doi: 10.1016/j.measurement.2010.11.015.
[29] C. Dimas, P. P. Sotiriadis, and A. H. Architecture, "Electrical Impedance Tomography Image Reconstruction for Adjacent and Opposite Strategy using FEMM and EIDORS Simulation Models," *2018 7th Int. Conf. Mod. Circuits Syst. Technol.*, 2018, pp. 1-4, doi: 10.1109/MOCAST.2018.8376604.
[30] R. S. Lotti, A. W. Machado, Ê. T. Mazzieiro, and J. Landre Júnior, "Aplicabilidade científica do método dos elementos finitos," *Rev. Dent. Press Ortod. e Ortop. Facial*, vol. 11, no. 2, pp. 35-43, 2006, doi: 10.1590/s1415-54192006000200006.
[31] B. Li, J. M. Wang, Q. Wang, X. Duan, and X. Li, "An Improved Generalized Finite Element Method for Electrical Resistance Tomography Forward Model," *J. Electr. Eng. Technol.*, vol. 14, no. 6, pp. 2595-2606, 2019, doi: 10.1007/s42835-019-00288-6.
[32] N. J. Avis and D. C. Barber, "Incorporating a priori information into the Sheffield filtered backprojection algorithm," *Physiol. Meas.*, vol. 16, no. 3A, 1995, doi: 10.1088/0967-3334/16/3A/011.
[33] A. Adler *et al.*, "GREIT: A unified approach to 2D linear EIT reconstruction of lung images," *Physiol. Meas.*, vol. 30, no. 6, 2009, doi: 10.1088/0967-3334/30/6/S03.